Heliyon 9 (2023) e15675

Contents lists available at ScienceDirect

Heliyon

journal homepage: www.cell.com/heliyon

Research article

Coupling effect of critical properties shift and capillary pressure on confined fluids: A simulation study in tight reservoirs

Yuhua Ma [a], Zhihong Kang [a], Xin Lei [a], Xiaodong Chen [b], Congbo Gou [b,c], Zhijiang Kang [d], Shuoliang Wang [a,*]

[a] School of Energy Resources, China University of Geosciences, Beijing, 100083, China
[b] Research Institute of Exploration and Development of Changqing Oilfield, PetroChina, Xi'an, 710000, Shaanxi Province, China
[c] Nation Engineering Laboratory for Exploration and Development of Low Permeability Oil and Gas Field, Xi'an, 710000, Shaanxi Province, China
[d] Sinopec Petroleum Exploration and Development Research Institute, Beijing, 100083, China

ARTICLE INFO

Keywords:
Compositional numerical simulation
Confined effect
Phase behavior
Critical properties shift
Capillary pressure

ABSTRACT

Critical properties shift and large capillary pressure are important contributors for the phase behavior altering of nanopore fluid. However, the effects of critical properties shift and large capillary pressure on the phase behavior are ignored in traditional compositional simulators, leading to inaccurate evaluation results of tight reservoirs. In this study, phase behavior and production of confined fluid in nanopores are studied. First, we developed a method for coupling the effect of critical properties shift and capillary pressure into the vapor-liquid equilibrium calculation base on Peng-Robinson equation of state. Second, a novel fully compositional numerical simulation algorithm considering effect of critical properties shift and capillary pressure on phase behavior is accomplished. Third, we have discussed the alterations of critical properties shift effect, capillary pressure effect and coupling effect on the composition of oil and gas production in detail. The critical properties shift and capillary pressure effects on oil and gas production in tight reservoirs are analyzed quantitatively through four cases, and the influences of the two effects in oil/gas production are compared. Based on the fully compositional numerical simulation, the simulator can rigorously simulate the impacts of component changes during production. The simulation results show that both the critical properties shift effect and the capillary pressure effect reduce the bubble point pressure of Changqing shale oil, and the influence are more prevalent in pores of smaller radius. In pores is larger than 50 nm, the phase behavior altering of the fluid can be ignored. In addition, we devised four cases to comprehensively investigate the effects of critical properties shift and large capillary pressure on production performance of tight reservoirs. The comparisons between the four cases show that the capillary pressure effect impacts the reservoir production performances greater than the critical properties shift effect, such as higher oil production, higher GOR, and lower content of lighter component and higher content of heavier component in the residual oil/gas. The results of coupling effects indicate that the critical properties shift effect would suppress the effect of the capillary pressure effect. In particular, the difference between the simulation results of the coupling effects and the base case is smaller than that between the simulation results of the capillary pressure effect and the base case.

* Corresponding author. Petroleum Engineering, China University of Geosciences, China.
E-mail addresses: mayh95@163.com (Y. Ma), wangshuoliang@cugb.edu.cn (S. Wang).

https://doi.org/10.1016/j.heliyon.2023.e15675
Received 8 November 2022; Received in revised form 8 April 2023; Accepted 18 April 2023
Available online 23 April 2023

1. Introduction

With the technological innovations in the past few decades, tight reservoirs with abundant original oil in place have aroused strong interests for production and have been further developed and utilized [1]. However, the production of tight reservoirs still faces multiple challenges [2–4]. Tight reservoirs are characterized by low porosity [5], low permeability [6,7] and narrow pore radius [6–11]. One of the most important factors in the evaluation of tight reservoirs is the phase behavior of fluids (hereafter referred to as "confined fluids"), which induces obvious deviations from the bulk fluids [12–14]. To understand the phase behavior of confined fluids better, some researchers conducted experiments [15–17] and suggested that the phase behavior of confined fluids differs from that of bulk fluids a lot due to the different intrinsic interactions between fluids and the pore wall [18–21]. According to recent research, some effects are thought to affect the phase behavior of nanofluids, such as capillary pressure [10,22,23], critical properties shift [24–27], adsorption [28–31], interfacial tension [9,32], pore shape [33,34] and pore wall roughness, etc. Among them, capillary pressure and critical properties shift are more significant effects than others.

In order to modify the influence of the confined effect on the phase behavior and make the predicted results more accurate and compared with the experimental data, many models have been proposed to characterize the phase behavior of confined fluids. Travalloni et al. [35] has modified the van der Waals equation of state to predict critical points of mechanical stability for confined fluids. It is shown that the critical points of confined fluids depended on pore size with considering the molecule–molecule and the molecule–wall interactions. Nojabaei et al. [7] modified phase equilibrium equations only based on the consideration of capillary pressure effect. The results show that the PVT properties of Bakken oil shifts apparently in reservoirs with large amounts of small pores. Subsequently, Telku et al. [23] coupled the capillary pressure and the critical properties shift in the calculations of conventional vapor-liquid equilibrium (VLE) for nanopore fluids. The difference of the thermodynamic properties between confined fluids and bulk fluids, such as bubble points, dew points, and IFT were studied. Furthermore, Chen et al. [36] developed a calculation method for upscaled phase behavior to account for competitive adsorption and capillary pressure in nanopores. It is reported that heavier components tend to reside in smaller pores and suppress the bubble point pressure which are calculated with considering capillary pressure and competitive adsorption. However, these models are only mathematical formulas calculating phase behaviors, examined the effect of capillary pressure on merely a portion of the phase envelopes, which cannot be directly applied in simulating the exploitation of unconventional reservoirs.

Although a large number of scholars have studied the factors affecting the phase behavior of confined fluids, there still lacks quantitative estimations of the relative influence of each factor. The influence of confined effects on reservoir evaluation is still not clear. Further works should be done to clarify the confined effects in the production of tight reservoirs. Specifically, to obtain accurate estimates, a reliable numerical simulator for shale and other tight reservoirs is required urgently.

Many recent modeling studies have focused on the differences in results due to confined effects of nanofluids [6,37,38]. These researches integrated capillary confinement based on the PVT measurements, pore size shrinkage due to compaction effect, pore throat size distribution and fluids saturation, shed light on some of the inconsistencies between the simulated and observed production, such as the discrepancies between the behaviors of gas-oil ratio (GOR) and oil production rate. However, in previous studies, the discussion is insufficient. Some scholars only discussed the influence of capillary pressure on the numerical simulation results, while others only discussed the influence of critical properties shift on the numerical simulation results. Considering the effect of capillary pressure in the calculation of VLE, Nojabaei et al. [7] gave a reduced bubble-point pressure and more accurate history matching of flow rate for the Bakken shale. Wang et al. [39] presented a compositional numerical simulator calculating the effect of capillary pressure on VLE with stability test and two-phase split flash calculation algorithms, and obtained lower bubble point pressure, liquid density and the oil viscosity results. The history matching of inconsistent GOR is also resolved. Similarly, in Siripatrachai's study [40] and our previous study [41], only the influence of capillary pressure on numerical simulation is discussed. Based on the results from these studies, it can be seen that considering capillary pressure into the calculation of VLE in numerical simulator will improve the reliability of recovery prediction.

On the other hand, critical properties shift is also an important factor affecting the phase behavior of nanofluids. As early as 1970, the influence of critical properties shift on phase behavior has been studied for a long time. However, few scholars have combined critical properties shift and capillary pressure into numerical simulators. As for the coupling effects of Capillary pressure and critical properties shift in the phase behavior of nanofluids, Li and Sheng [42] discussed the influence of critical properties shift and capillary pressure on the phase envelope curve of multicomponent fluids. Furthermore, Zhang et al. [43] integrated the effects of both the critical properties shift and capillary pressure into a black oil numerical simulator. However, in the black oil model, the change of capillary pressure with the composition of fluids in production is neglected. When using Young-Laplace equation to calculate capillary pressure, densities of the liquid, vapor phases, and mole fractions of components in the liquid and vapor phases are indispensable, and these parameters need to be iterated into the calculation of phase equilibrium. Therefore, it is necessary for the fully compositional numerical simulator to consider the influence of capillary pressure and critical properties shift into the calculation of VLE for tight reservoirs.

Capillary pressure and critical properties shift play important roles in changing the phase behavior of confined fluids. These two effects exhibit different dominant positions in reservoir development and different effects on different reservoir components. In order to obtain the basic principles and quantitative results of the two coupled effects in different reservoirs, we need to understand how a single effect or combined effects impact the phase behavior of confined fluids, and further how it impacts the numerical simulation results. This shows important implications for improving field operation strategies meanwhile enhances the reliability of recovery predictions.

In this work, we evaluated the influences of confined effects on tight reservoir production from the perspective of capillary pressure and critical properties shift. First, the specific modification of the VLE calculation considering critical properties shift and capillary pressure is described. The influence of critical properties shift and large capillary pressure on phase behavior of hydrocarbon mixtures is discussed. Then, a reservoir model is established according to the geological data of Changqing oilfield shale reservoir, and the confined effect is added to the numerical simulation. Finally, the sensitivities of parameters are analyzed. The effects of capillary pressure, critical properties shift and their coupling on production parameters such as saturation, oil and gas production and composition are quantitatively compared for the first time.

2. Methodology

The compositional simulator simulates the changes of fluid components and distribution more accurately than black oil simulator during the exploitation and development. Thus, in this study, we developed a fully implicit reservoir compositional simulator and integrated the influence of critical properties shift and capillary pressure into the calculation of vapor/liquid phase equilibrium to compare the influences of confined effects on the phase behavior of nanofluid. In this section, the evaluation of the critical properties shift and the capillary pressure are presented, and the method for coupling the two effects into the VLE calculation are described.

2.1. Evaluation of critical properties shift

The critical properties of hydrocarbon components in nanopores vary with pore size [44], and the correlation formula of critical properties shift and pore size were proposed by Zhang et al. [45,46], Alharthy et al. [8] and Zarragoicoechea et al. [47], respectively. We compared and analyzed these two correlation formulas:

On the one hand, in Zhang's method [45,46], two generalized analytical formulations considering the critical temperature and critical pressure shift for fluid adsorption in nanopores are initially proposed on the basis of modified van der Waals and SRK EOSs.

On the other hand, in Alharthy's method [8], the shift of critical properties is only related to the pore radius and the critical properties of pure component in bulk. The shift in critical pressure is not correlated with the critical temperature, and similarly the shift in critical temperature is not correlated with the critical pressure.

$$\begin{cases} \dfrac{\Delta P_c}{P_{cb}} = -0.4097d + 1.2142 \\ \ln\left(\dfrac{\Delta T_c}{T_{cb}}\right) = 0.093764 - 0.929d \end{cases} \quad \text{Equation 1}$$

where T_{cb} and P_{cb} are the critical temperature (K) and critical pressure (Pa), ΔT_c and ΔP_c are the shift of the critical temperature and critical pressure in the pores from that in bulk; d is the pore diameter (m).

In Zarragoicoechea's method [47], the relationship between the shift of critical properties and Lennard-Jones impact diameter (σ_{LJ}) and pore radius (r_p) are developed base on the critical temperature and pressure shift of argon, xenon, carbon dioxide, oxygen, nitrogen and ethylene in McM-41:

$$\begin{cases} \Delta T_c^* = \dfrac{T_{cb} - T_{cp}}{T_{cb}} = 0.9409\dfrac{\sigma_{LJ}}{r_p} - 0.2415\left(\dfrac{\sigma_{LJ}}{r_p}\right)^2, \\ \Delta P_c^* = \dfrac{P_{cb} - P_{cp}}{P_{cb}} = 0.9409\dfrac{\sigma_{LJ}}{r_p} - 0.2415\left(\dfrac{\sigma_{LJ}}{r_p}\right)^2, \\ \sigma_{LJ} = 0.244\sqrt[3]{\dfrac{T_{cb}}{P_{cb}}} \end{cases} \quad \text{Equation 2}$$

where r_p is the pore radius (nm) , T_{cb} and T_{cp} are the critical temperature of bulk fluids (K) and the critical temperature of confined fluids (K) , σ_{LJ} is Lennard-Jones collision diameter (nm) , P_{cb} and P_{cp} are the critical pressure of bulk fluids (atm) and the critical pressure of confined fluids (atm).

Compared with equation (2), equation (1) cannot represent bulk phase when the pore diameter is infinite; in addition, equation (2) matched well with the experimental data [48] and the Grand Canonical Monte Carlo (GCMC) simulation results [44]. Furthermore, in this study the Peng-Robinson equation of state (PR-EOS) [49] is used. Therefore, equation (2) was applied in this study.

2.2. Evaluation of capillarity effect

The capillary pressure is determined by the pore geometry and the wettability of the rock surface. The classical method can be applied in nanopores, presenting as below.

When calculating the capillary pressure between oil and gas, it is assumed that the reservoir is oil wet, thus the gas phase pressure can be expressed as:

$$P_V = P_L + P_{cap} \quad \text{Equation 3}$$

The capillary pressure is calculated according to Young Laplace equation:

$$P_{cap} = \frac{2\sigma \cos\theta}{r_p} \quad \text{Equation 4}$$

where P_{cap} is capillary pressure (Pa); σ is interfacial tension (IFT) between vapor and liquid phase (N/m); θ is the contact angle (assumed to be 45° in this study) , and r_p is radius (nm); σ is calculated using the following relationship established by MacLeod and Pedersen [50,51]:

$$\begin{cases} \sigma = (P_L\overline{\rho}_L - P_V\overline{\rho}_V)^v \\ P_L = \sum_{i=1}^{Nc} x_i P_i \\ P_V = \sum_{i=1}^{Nc} y_i P_i \end{cases} \quad \text{Equation 5}$$

where v is the scaling exponent, $v = 3.6$; $\overline{\rho}_{L/V}$ is the average molar density of bulk liquid/vapor phases (mole/cm^3); x_i and y_i are the mole fraction of component i for liquid and vapor phases, respectively; P_i is the parachor of liquid/vapor phases:

$$P_i = (8.21307 + 1.97473\omega_i)T_{ci}^{1.03406}P_{ci}^{-0.82636} \quad \text{Equation 6}$$

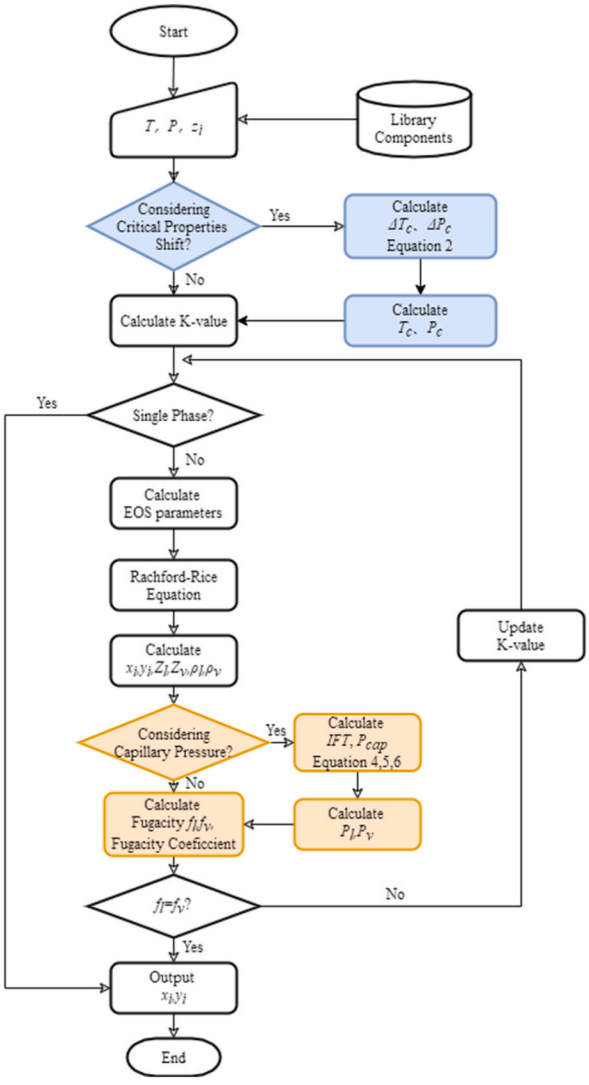

Fig. 1. Workflow for modified vapor/liquid-phase equilibrium calculation.

where ω_i is the acentric factor , T_{ci} is critical temperature (K), P_{ci} is critical pressure (bar).

According to equations (4) and (5), the capillary pressure depends on the density and composition of oil and gas phase, which are obtained by Newton iterations in phase equilibrium calculation.

Therefore, in this study, the calculation of capillary pressure is added to the Newton iteration of phase equilibrium. The capillary pressure (P_{cap}) between the gas and the oil phase is calculated by solving the objective function iteratively as shown in the workflow of Fig. 1. Firstly, initial guess value (P_{cap} = 500 Pa) for the initial capillary pressure was set. In each iteration cycle, the density and composition of oil and gas phase are calculated, and then the IFT and capillary pressure. Subsequently, the newly obtained capillary pressure is used as the input parameter to calculate the pressure and fugacity of oil and gas phase. Finally, whether the phase equilibrium converges or not are determined. If the converges are obtained, the phase equilibrium calculation is cut off. If it does not converge, K-value is updated and the Newton iteration process are repeated until it converges.

2.3. Modification of VLE calculation

The improved process based on the classical flow of the VLE calculation are presented in this section. The main modifications involve the consideration of (I) critical properties shift and (II) capillary pressure in the calculation of VLE. Fig. 1 shows a modified workflow for VLE calculations with coupled critical properties shift or capillary pressure effect. The detailed description is as follows：

(I) Critical properties shift. As shown in the blue frames in Fig. 1, at the beginning of the calculation, the critical properties are required to determine whether this shift effect should be considered when the fluid critical temperature (T_c) and critical pressure (P_c) are input. The Peng-Robinson equation of state (PR-EOS) [49] are used for calculating VLE:

$$P = \frac{RT}{V-b} - \frac{a}{V(V+b)+b(V-b)} \quad \text{Equation 7}$$

where P is pressure (MPa); T is temperature (K); V is molar volume (m^3/kmol); R is gas constant; a and b are parameters of PR-EOS.

For confined fluid in nanopores, the parameters of PR-EOS are rewritten as:

$$a = 0.45724 \frac{R^2\left[\left(1-\Delta T_c^*\right)T_c\right]^2 \alpha(\mathrm{T})}{\left(1-\Delta P_c^*\right)P_c} \quad \text{Equation 8}$$

$$\mathrm{b} = 0.07780 \frac{R\left(1-\Delta T_c^*\right)T_c}{\left(1-\Delta P_c^*\right)P_c} \quad \text{Equation 9}$$

where $\alpha(T) = \left[1+k\left(1-\left[\frac{T}{(1-\Delta T_c^*)T_c}\right]^{0.5}\right)\right]^2$; k is the constant property of each substance. The correlation equation is: $k = 0.37464 + 1.54226\omega - 0.26992\omega^2$, where ω is the eccentricity factor.

For a fluid mixture, the van der Waals mixing rule is used for calculating constants a and b.

$$a_m = \sum_i \sum_j x_i x_j \left(a_i a_j\right)^{0.5} 1-\delta_{ij} \quad \text{Equation 10}$$

$$b_m = \sum_{i=1}^{n} x_i b_i \quad \text{Equation 11}$$

where x_i, x_j is the mole fraction of component i, j; a_i, a_j and b_i are parameters of PR-EOS for pure component i,j; δ_{ij} is the binary interaction coefficient of components i and j.

(II) Capillary pressure. As shown in the orange frames in Fig. 1, capillary pressure is evaluated before calculating the fugacity to determine if this effect should be considered. It can be revealed by adding the gas phase partial pressure (P_V) to the VLE calculations. To solve the PR-EOS containing the gas-phase pressure and the liquid-phase pressure, the parameters A_L、 B_L、 A_V and B_V are set. For a mixture, the PR-EOS is rewritten as:

$$Z_L{}^3 - (1-B_L)Z_L{}^2 + \left(A_L - 3B_L{}^2 - 2B_L\right)Z_L - \left(A_L B_L - B_L{}^2 - B_L{}^3\right) = 0 \quad \text{Equation 12}$$

$$Z_V{}^3 - (1-B_V)Z_V{}^2 + \left(A_V - 3B_V{}^2 - 2B_V\right)Z_V - \left(A_V B_V - B_V{}^2 - B_V{}^3\right) = 0 \quad \text{Equation 13}$$

where

$$A_L = \frac{aP_L}{R^2T^2}A_V = \frac{aP_V}{R^2T^2}B_L = \frac{bP_L}{RT}B_V = \frac{bP_V}{RT}$$

According to Gibbs' free energy principle, the smallest real root is solved as the liquid-phase compression factor Z_L and the largest real root as the vapor-phase compression factor Z_V.

Furthermore, Z_L, Z_V are substituted into the fugacity coefficient ($\varnothing^i$) equation:

$$\ln \varnothing_V^i = \frac{b_i}{b_m}(Z_V - 1) - \ln(Z_V - B_V) - \frac{Z_V}{2\sqrt{2}B_V}\left(\frac{2\sum_{j=1}^{N} x_j a_{ij}}{a_m} - \frac{b_i}{b_m}\right)\ln\left[\frac{Z_V + (1+\sqrt{2})B_V}{Z_V + (1-\sqrt{2})B_V}\right] \quad \text{Equation 14}$$

$$\ln \varnothing_L^i = \frac{b_i}{b_m}(Z_L - 1) - \ln(Z_L - B_L) - \frac{Z_L}{2\sqrt{2}B_L}\left(\frac{2\sum_{j=1}^{N} x_j a_{ij}}{a_m} - \frac{b_i}{b_m}\right)\ln\left[\frac{Z_L + (1+\sqrt{2})B_L}{Z_L + (1-\sqrt{2})B_L}\right] \quad \text{Equation 15}$$

where $\varnothing_V^i$ and $\varnothing_L^i$ are fugacity coefficient of vapor and liquid phases for a mixture; a_m and b_m are parameters of PR-EOS for a mixture in Equation (10) and (11).

The fugacity can be calculated by:

$$f = z_i \varnothing^i P \quad \text{Equation 16}$$

where z_i is the mole fraction of component i.

To determine whether the gas phase fugacity f_V and liquid phase fugacityf_L are in equilibrium :

$$| f_L(T,P,x) - f_V(T,P,y) | < 10^{-5} \quad \text{Equation 17}$$

where f_L is the fugacity of the components in the liquid-phase, f_V is the fugacity of the components in the vapor-phase.

According to thermodynamics, when the gas phase fugacity is equal to the liquid phase fugacity, the equilibrium of the vapor and liquid phases is achieved.

3. Reservoir simulation

Tight reservoirs or shale reservoirs are featured by extremely low porosity and permeability. In the process of primary oil recovery, there are large amount of oil trapped in small pores [52]. The production relied on nature energy depletion, such as Changqing Oilfield in China, where the oil recovery rate of most single wells decreases rapidly, and the recovery rates reach very low levels [53,54]. For conventional reservoirs, water flooding is a common method to maintain formation pressure. However, for tight oil reservoirs, the water-flooding could not improve the oil recovery effectively, and the oil sweep efficiency is very hard to improve. Gas injection is the promising method to improve oil recovery. Moreover, tight reservoirs have a better CO2 reservoir storage performance due to their extremely small pore size than the conventional reservoirs. The maximum storage height and storage capacity can be optimized in shale reservoirs by considering the nanoconfined effect [55]. In this study, a fully implicit reservoir compositional simulator is used to simulate the oil production for a CO2 flooding process in tight reservoir.

3.1. Multi-components mixtures

The fluids type applied in the numerical simulation is a multi-components mixtures of shale oil from the well XP-2 in Changqing Oilfield, China. The component composition, basic properties and the binary interaction parameters coefficients are listed in Tables 1 and 2.

3.2. Reservoir model parameters

We established a simple cubic reservoir model. The model includes 5000 grids, 5 vertical wells and a hydraulic fracture. The reservoir parameters are shown in Table 3. As shown in Fig. 2, five vertical wells form a five point well pattern, a production well at the middle of the reservoir and four injection wells at the middle of the reservoir. The production well is produced under constant pressure (3 MPa) for 1600 days, and CO2 gas is injected into the injection well at constant rate (400 m^3/day) for 1200 days.

Table 1
Component properties of the fluids mixtures.

Component	*Pc* (MPa)	*Tc* (K)	Acentric fact (unitless)	Mol. Weight (g/mol)	Zi (%)
CO2	7.3866	304.7	0.225	44.010	1.2
CH4	4.6042	190.6	0.008	16.043	38.7
C2H6toNC4	4.4479	353.0	0.135	40.073	19.4
C5toC7	3.2337	518.4	0.286	88.287	11.9
C8toC12	2.7371	596.7	0.393	120.188	23.5
C13toC20	1.8091	724.0	0.659	212.091	4.1
C21toC36	1.2224	829.6	0.956	333.462	1.2

Table 2
Binary interaction parameters for fluids mixtures.

	CO2	CH4	C2H6toNC4	C5toC7	C8toC12	C13toC20	C21toC36
CO2	0	0.105000	0	0	0	0	0
CH4	0.105000	0	0.006552	0.026504	0.039073	0.068651	0.096291
C2H6 to NC4	0	0.006552	0	0.006911	0.014147	0.034461	0.055802
C5 to C7	0	0.026504	0.006911	0	0.001312	0.010894	0.024543
C8 to C12	0	0.039073	0.014147	0.001312	0	0.004686	0.014699
C13 to C20	0	0.068651	0.034461	0.010894	0.004686	0	0.002841
C21 to C36	0	0.096291	0.055802	0.024543	0.014699	0.002841	0

Table 3
Reservoir model parameters.

Parameters	Value
Reservoir dimension	25*25*8
Grid size	40*40*5 m
Formation thickness	5 m
Initial reservoir temperature	60 °C
Initial reservoir pressure	15 MPa
Porosity	8%
Matrix permeability	$10 \times 10^{-3}\mu m^2$
Fracture permeability	$1000 \times 10^{-3}\mu m^2$
Initial water saturation	35%
Initial oil saturation	65%
Number of components	7
Number of wells	5
Injection well specification	Constant RATE: $400 m^3$/day
Production well specification	Constant BHP: 3 MPa

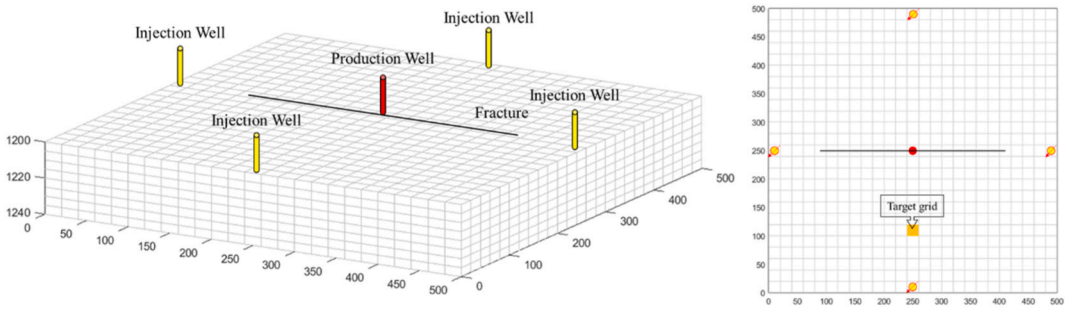

Fig. 2. Three-dimensional and vertical view of a five point well pattern model with a hydraulic fracture.

The relative permeability curve of oil-water is shown in Fig. 3(a), and the relative permeability curve of liquid-gas is shown in Fig. 3 (b). The oil phase can only transition with the gas phase, and the sum of oil, gas and water saturation is 1.

3.3. Cases

In this study, we designed four different cases, based on which the coupling effect of capillary pressure (10 nm) and critical properties shift in phase equilibrium calculation can be compared quantitatively. They are:

(1) Base Case

In the calculation of gas-liquid equilibrium, the commercial numerical simulation software ignores the effect of confining effect on the phase behavior of nano-pore fluids. Thus, neither the capillary pressure nor the critical properties shift is considered.

(2) A case where the capillary pressure is considered in phase equilibrium (PC case)

The capillary pressure is calculated by Young-Laplace equation in the calculation of gas-liquid equilibrium. In the calculation of the vapor/liquid-phase equilibrium, the gas phase pressure is added into the PR equation of state. The specific calculation process has been described in equations (3)–(5).

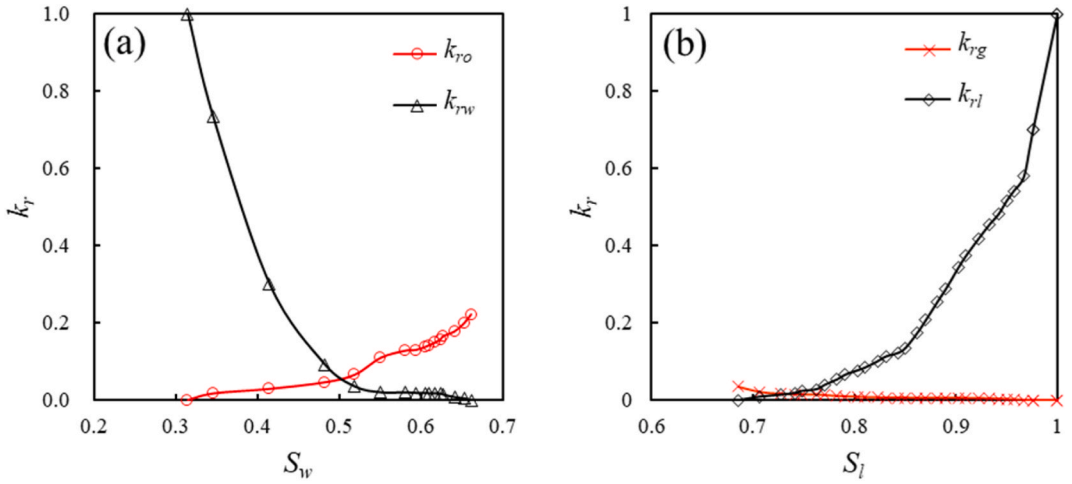

Fig. 3. Relative permeability curve for (a) oil-water phase and (b) liquid-gas phase.

(3) A case where the critical properties shift is considered in phase equilibrium (CPS case)

The critical properties shift is considered in the vapor/liquid-phase equilibrium calculation, and the critical properties shift is calculated by equation (2).

(4) A case where the critical properties shift and capillary pressure are combined in calculating phase equilibrium (CPS&PC case)

Both the capillary pressure and the effect of critical properties shift are considered. In the initial input of pure component properties, the confined critical temperature and pressure are used. In the vapor/liquid-phase equilibrium calculation, the capillary pressure calculated by Young-Laplace equation was added to PR equation of state.

4. Results and discussions

4.1. Confined phase behavior

4.1.1. Critical properties shift

As shown in Fig. 4 (a) and (b), the absolute shift of critical temperature and pressure for each pure component (Table 1) of the XP-2 shale oil mixture are presented according to different pore radius based on equation (2). Obviously, the critical temperature and

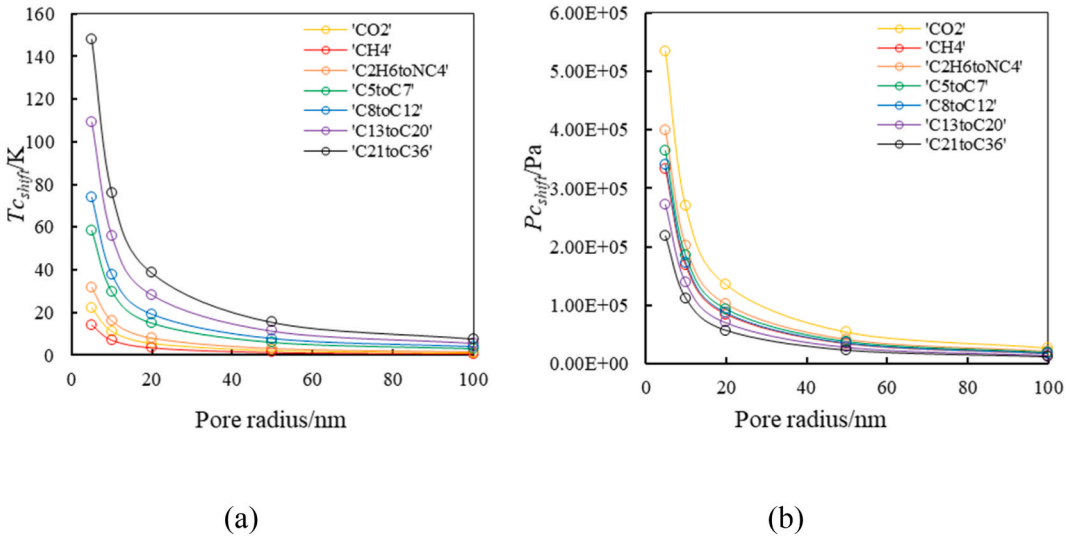

Fig. 4. (a)Critical temperature of pure component vs. pore radius; (b) Critical pressure of pure component vs. pore radius.

pressure shifts both increase with decreased pore width, especially at r_p less than 50 nm. For example, with r_p changing from 50 to 5 nm, the reduction of critical T and P increased at least 15 and 2E5 times of the initial levels, respectively. Nevertheless, with r_p changing from 100 to 50 nm, the alters of the critical properties are so small (1–5 times) that can be ignored.

In pores at the same size, the absolute reduction of critical temperature for heavy components is greater, whereas those of the critical pressure are usually lower than that of the light components. The absolute reduction in the critical pressure of CH4 is an exception, which is far less than the *Pc* variation of CO2, plotted close to C8–C12, which may be related to the fact that the critical pressure of CH4 bulk fluids is smaller than that of CO2 bulk fluids.

Fig. 5 shows the dimensionless critical pressure shift and the critical temperature shift of pure components in the XP-2 shale oil calculated from Equation (2) at different pore radius. It can be demonstrated that for all the pure components in the legend, the relative shift of critical properties increases with decreased pore radius. At the same pore radius, the greater the molar molecular weight of components is, the greater the *Tc/Pc* shift is, according to which the data values of CH4 and CO2 are almost the same. Namely, the critical properties shift effect is more prevalent in reservoirs with smaller pore size and heavier fluid components..

Fig. 6 shows the critical temperature and pressure of pure CO2 component, pure CH4 component and pseudo C21–C36 component in different sizes of pores (radius = 5, 10, 20, 50 and 100 nm). The data points of different components from distinct groups, while the points of the same component cluster close no matter what the pore sizes are. For the total three data clusters, with pore size ranging from 100 nm to 5 nm, both Tc and *Pc* decrease, inducing a shifting trend to the lower left corner in the P_c-T_c figure. Since the distances between the points for r_p is 5 nm (red) and 10 nm (orange) are farther than that between r_p is 50 nm (blue) and 100 nm (black), the P_c and T_c shifts are larger in smaller pores, impling that the critical properties shift in nano-pores are more apparent. Besides, the comparison of the data point distance and distribution between the three groups of data shows that the heavier the fluid components are, the greater the shifts appear.

Since the critical property parameters of components need to be used in the calculations of the VLE, the critical properties shift of confined fluids will inevitably affect the phase envelope of fluids. As shown in Fig. 7, the bubble point envelopes of confined fluids (5–100 nm) all plot different from the bulk fluids (INF). It shows that the smaller the pore radius is, the smaller the bubble point pressure is. At reservoir temperature, the relative reduction between the bubble point pressure for r_p equal 100 nm, 50 nm and 5 nm and the bubble point pressure for r_p equal INF is 0.7%, 2.1% and 14.1%, respectively. It indicates that the shift of critical properties in pores larger than 50 nm is slight that can be ignored in most circumstances. The shift of bubble point pressure is also related to temperature. Although the increasing trends of the bubble point pressure for r_p ranging from 5 to 100 nm are similar with temperature alters, the divergence between them increased obviously, especially for the curves represent smaller r_p. In summary, at high the temperature is, the more the bubble pressure reduces. At low temperature, the shift of critical properties has little effect on phase behavior.

4.1.2. *Vapor/liquid-phase equilibrium calculation considering capillary pressure*

Fig. 8 shows the bubble point envelopes of XP-2 shale oil confined fluids at different pore radius. The bubble point pressure of nanofluids with different pore sizes increases with increasing temperature in the temperature ranging from 273.15 to 453.15K, but the increasing rate is gradually decreasing. Moreover, the pore radius will affect the bubble point pressure. The smaller the pore radius, the greater the capillary pressure, and the greater the impact on the bubble point pressure. For example, at reservoir temperature, the bubble point pressure in a pore with a radius of 5 nm is about 5.8 MPa, which is 58.3% smaller than that of 13.9 MPa in a pore with a radius of 100 nm. In addition, high temperature suppresses the effect of pore radius on bubble point pressure. At 423.15 K above the reservoir temperature, the difference value between the bubble pressure in the pore with a radius of 5 nm and 100 nm decreases from 8.1 MPa to 2 MPa. The reason for this trend is that at critical point, the density of the liquid phase and gas phase are the same, thus IFT is 0, and the capillary pressure disappears. Therefore, when the temperature and pressure is close to the critical point, the capillary pressure effect on the phase behavior of the confined fluids becomes subtle. Also note that the phase equilibrium calculation of confined fluids in small pore radius (less than 5 nm) is challenging at low bubble point pressure. When the pore radius is less than 5 nm,

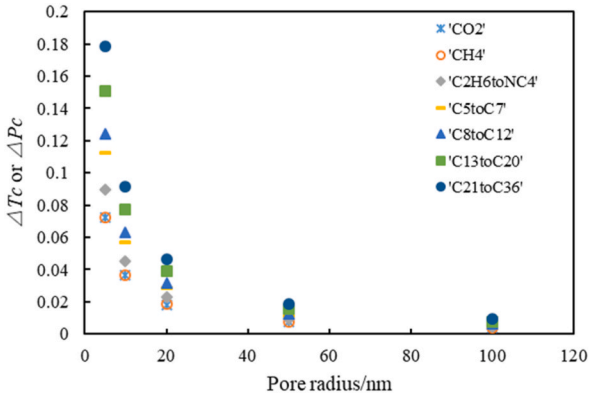

Fig. 5. Dimensionless critical pressure shift and the critical temperature shift of pure component vs. pore radius.

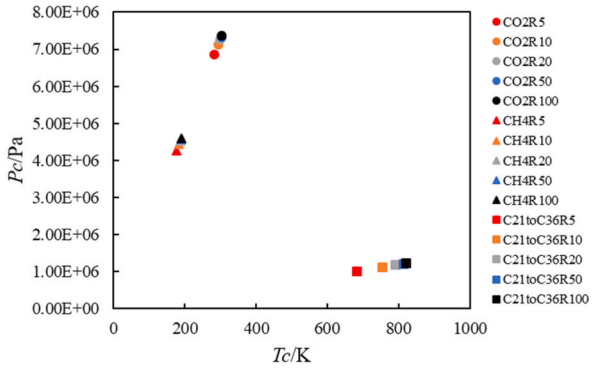

Fig. 6. Critical-temperature and –pressure of pure component vs. pore radius.

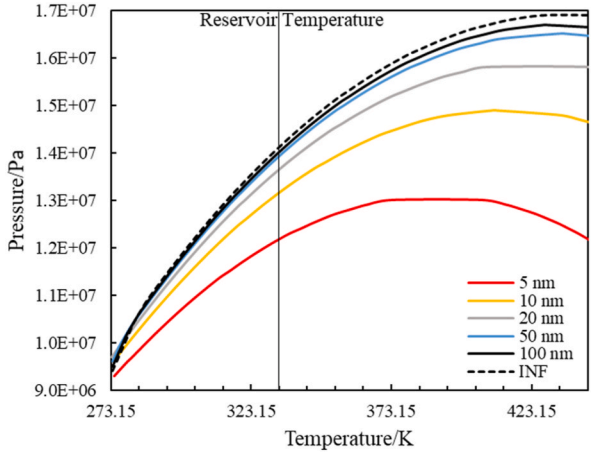

Fig. 7. Bubble point pressure of XP-2 shale oil considering critical properties shift effects at different pore radius.

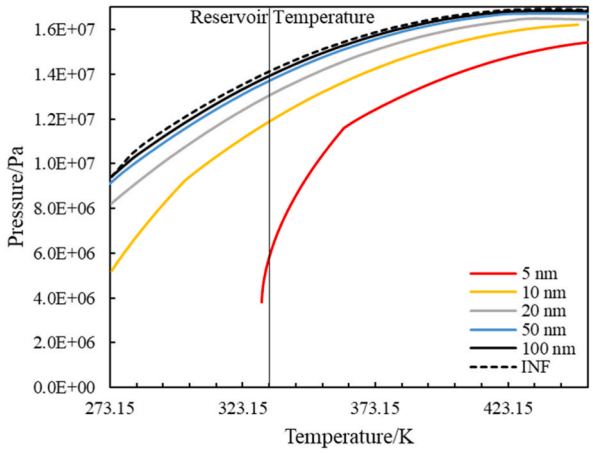

Fig. 8. Bubble point pressure of XP-2 shale oil considering capillary pressure effects at different pore radius.

the capillary pressure is extremely large, even higher than the bubble point pressure. In this case, whether the influence of capillary pressure on the confined fluids phase behavior is correct is worth considering.

4.1.3. Combined critical-properties shift and capillary pressure effect

Fig. 9 shows the envelope line of XP-2 shale oil bubble point obtained on the basis of different factors under the condition of pore

radius of 10 nm: (a) the dotted line in the figure represents unrestricted fluids, i.e. bulk-phase behavior; (b) the solid yellow line in the figure represents the case influenced only by the critical properties shift; (c) the solid blue line in the figure represents the case affected only by capillary pressure; (d) the solid red line in the figure represents the case affected by the shift of combined fluids critical properties and capillary pressure.

Compared to (a), (b) in the higher temperature region, the bubble point pressure is obviously lower, while in the lower temperature region, it is close to the values of case (a). While the capillary pressure results in obvious lower bubble point pressure at lower *T* region, whereas close to case (a) at higher *T* region. Thus, the coupling effects of critical properties shift (c) and capillary pressure (d) gives lower bubble point pressure values than that from the respective effect when the temperature exceeds 300 K. When the reservoir temperature is below 300 K, the bubble point pressure only affected by capillary pressure are the lowest among all the cases in Fig. 9. In other words, the shift of critical properties at low temperature region will inhibit the influence of capillary pressure. At 383.5 K, the critical properties shift (c) and capillary pressure (d) cause the same decrease to the bubble point pressure of the confined fluids (only take XP-2 shale oil as an example).

4.2. Reservoir simulation

In this section, the fluids saturation, cumulative oil production, cumulative gas production, production gas-oil ratio, and composition changes for the four cases are analyzed and compared in detail, respectively. The original state of reservoir fluids is single-phase oil with an initial oil saturation of 0.65 and gas saturation of 0.

4.2.1. The influence of confined effect on fluid saturation

The four-color curves in Fig. 10(a) show the change of oil/gas saturation with time in a single grid of the four cases. A top view of the reservoir model is shown in Fig. 2 to show the location of the target grid. The production is divided into two stages: depletion production (0–1600days) and CO2 immiscible flooding (1600–2800 days). In depletion production stage, with the progress of production, the oil saturation of the four cases gradually decreased, with PC case having the highest oil saturation and CPS case having the lowest oil saturation. The 3D view of oil saturation fields after 40 days and 870 days in Fig. 11 can also be seen this trend. In addition, as shown in Fig. 10 (b), the oil saturation variation of PC case, CPS case and CPS&PC case were compared with that of Base case. It is shown that the oil saturation of PC case and CPS&PC case is 5.08% and 3.37% higher than that of Base case, respectively, while the oil saturation of the CPS case reservoir grid is 1.12% lower than Base case. After the process of CO2 injection, oil saturation firstly increases and then decreases, which is because CO2 injection plays a role of enhancing oil-displacement efficiency first. The inflection point appeared in the oil saturation curve at 1750 days, which was induced by CO2 breakthrough. It can be seen from Fig. 11 that the oil saturation first decreases near the gas injection well, then CO2 diffuses to the fractures, and finally the residual oil saturation remains relatively high only in the four corners of the reservoir. Comparing the oil saturation field after 2830 days, the residual oil saturation of Base case and CPS case is higher than that of PC case and CPS&PC case.

For gas saturation, the trend of the reservoir grid is reverse to that of the oil saturation. PC and CPS&PC cases show lower gas saturation than Base cases. As for the influence of the confined effect on the initial fluids phase behavior, the bubble point pressure in the Base case is the highest (Fig. 9), that is to say, the fluid in Base case is the easiest to degassing. However, the gas saturation in the CPS case was consistently higher than that in the Base case. This is inconsistent with the trend of bubble pressure shown in Fig. 8. This indicates that the saturation change of the reservoir is not only controlled by the phase behavior, but more complicated, which may also be related to the influence of the confined effect on the composition of components. In Fig. 9, the influence of the four cases on the initial fluids phase behavior of the same component is only calculated without considering that the component composition will change with production. It will be discussed later. As shown in Fig. 10 (c), in depletion production stage, the gas saturation variation of PC case, CPS case and CPS&PC case were compared with that of Base case, showing that the gas saturation of PC case and CPS&PC case

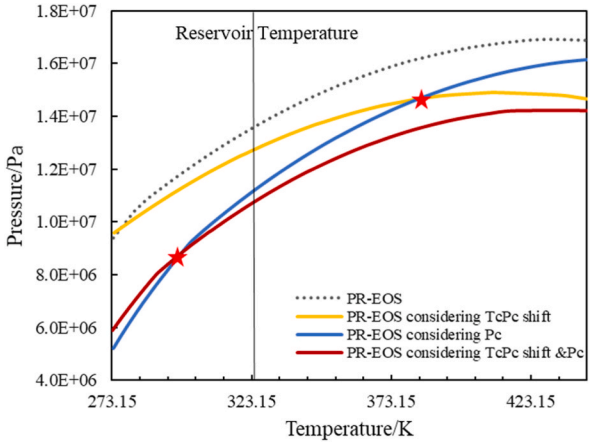

Fig. 9. Bubble point pressure of XP-2 shale oil with considering different effects and without at pore radius of 10 nm.

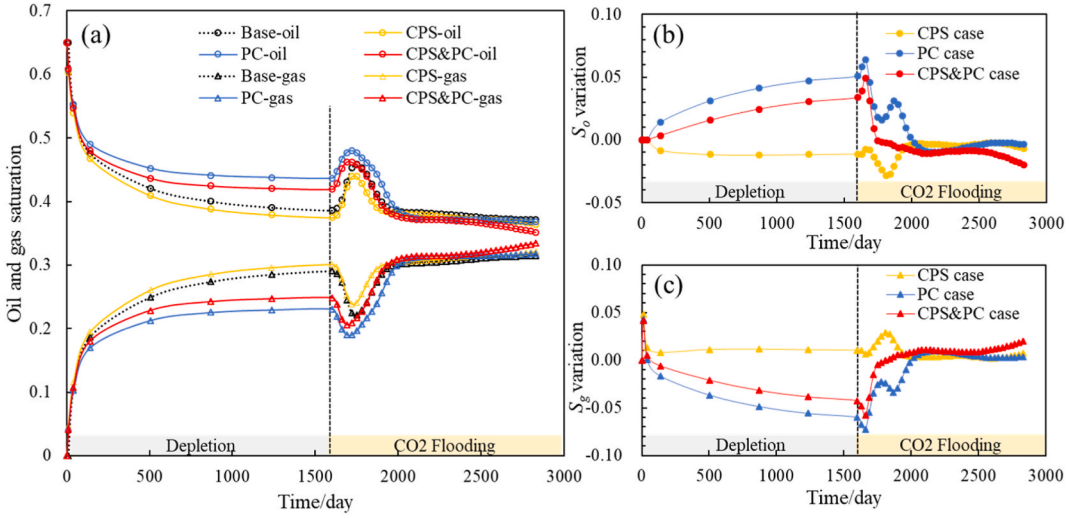

Fig. 10. (a) Oil/gas saturation of the reservoir grid; (b) Oil saturation variation of the reservoir grid; (c) Gas saturation variation of the reservoir grid.

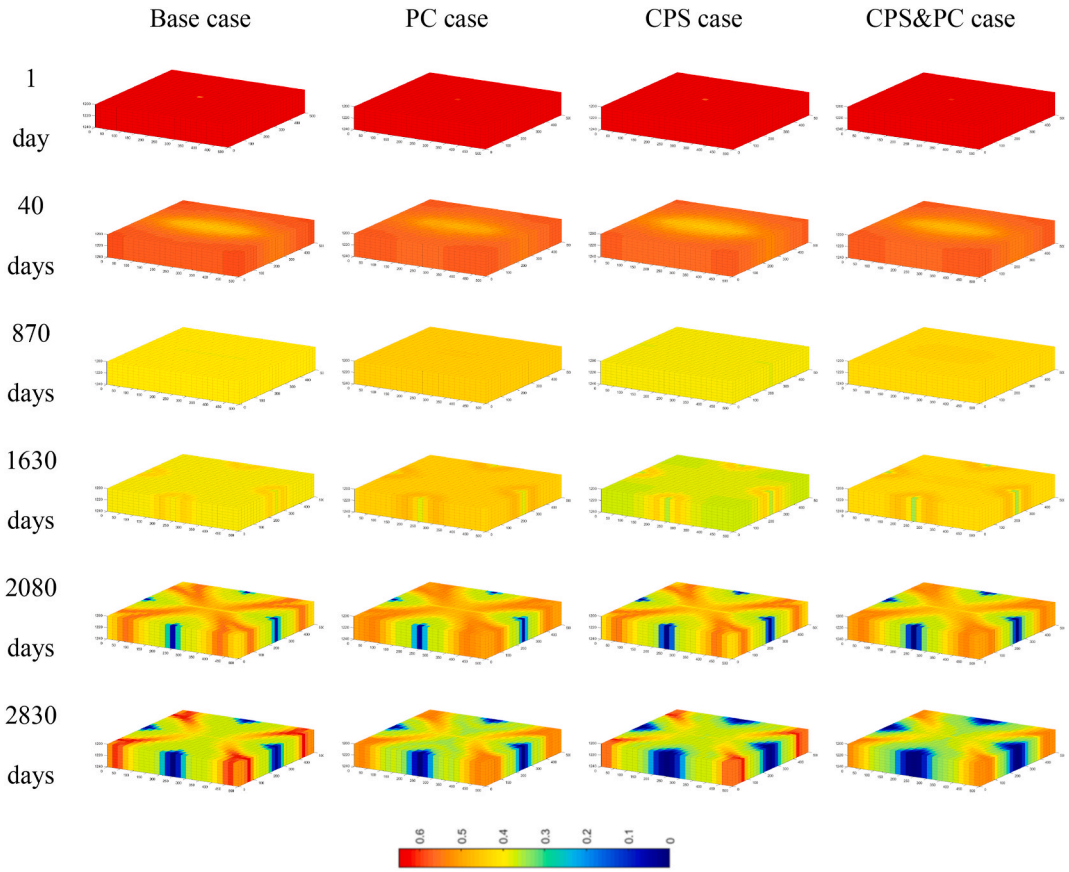

Fig. 11. Three-dimensional view of oil saturation fields for the four cases.

is 20.63% and 14.63% lower than that of Base case, respectively, while the gas saturation of the CPS case reservoir grid is 3.56% higher than Base case. After the process of CO2 injection, gas saturation increases. Finally, due to the breakthrough of CO2, the gas saturation of the four cases is close.

4.2.2. The influence of confined effect on cumulative oil/gas production

As shown in Fig. 12 (a), the cumulative oil production of the PC case, CPS case and CPS&PC case are higher than the Base case. The highest cumulative oil production is obtained in the CPS&PC case, which are 23.5% higher than the Base cases. In addition, during the early stage of CO2 flooding process (<690 days), the cumulative oil production of CPS case was higher than Base case, while CPS effect is unfavorable to oil production in the later stage of CO2 flooding. Compared with PC case and CPS case, it can be found that the capillary pressure effect had a positive effect on the oil increment (28.5%), while the critical properties shift effect produced an oil reduction (−4.1%).

Moreover, the gas production from the PC case and CPS&PC case are less than the Base case (Fig. 12 (b)), however, the critical properties shift effect causes higher gas production. CPS&PC case results show that the reduction effect of capillary pressure on accumulated gas is stronger than the increase of gas production caused by properties shift. In the CO2 injection stage, PC case shows the highest cumulative oil increase. At the end of CO2 gas injection flooding, the accumulated gas of the CPS case increased and accumulated oil decreased.

Fig. 13 shows the variation of production GOR with production time. The whole production is divided into two stages: depletion production and CO2 immiscible flooding. In the depletion production stage, the GOR of CPS case was much higher than that of the Base case, PC case and CPS&PC case. After CO2 injection, GOR of the four cases first decreased due to produces displacement and then increased rapidly after the breakthrough. In terms of the two stages of production, the effect of capillary pressure on GOR is more significant in depletion production stage, while in CO2 flooding stage, once CO2 breaks through, it is mainly affected by critical properties shift.

Among the four cases above, only the PC case and CPS&PC case require iterative calculation of the capillary pressure in the VLE. As shown in Fig. 14, the capillary pressure in the PC case is greater than that in CPS&PC case. Critical properties shift suppresses capillary pressure of oil and gas phases. In 10 nm pore, the capillary pressure is about 1.5 MPa when bubbles first time appear in reservoir. The capillary pressure gradually increased to 3.5 MPa during depletion production, which is related to the component changes during the production process, which will be discussed later. After CO2 injection, the capillary pressure decreases rapidly. Due to the low formation pressure of the reservoir, CO2 miscibility was not considered in the simulation process. The large amount of CO2 gas reduces the capillary pressure of oil and gas phases.

As shown in Fig. 15 (a)-(f), in order to estimate the effect of pore radius on production result, the cumulative oil/gas production of PC case, CPS case and CPS&PC case is compared at pore radius of 10 nm, 20 nm, 50 nm, 100 nm and infinity. The simulation results show that the cumulative oil production increases and the cumulative gas production decreases for the PC and CPS&PC instances as the pore radius decreases, while the cumulative oil production and the cumulative gas production decrease slightly for the CPS instance as the pore radius decreases. In both CPS and PC cases, the decreasing pore radius has a more significant effect on the cumulative hydrocarbon production. Compared with the 100 nm pore radius model, the cumulative oil production of the 10 nm pore radius model is about 8.9% higher, and the cumulative gas production is about 40% lower. The effect of confined effect on cumulative oil and gas production was negligible when the pore radius was extended to more than 50 nm. In addition, it can be seen from the comparison that capillary pressure is the dominant factor affecting the cumulative oil and gas production, and the effect of critical properties shift is less effective than capillary pressure.

4.2.3. The influence of confined effect on component composition

Fig. 16 (a)-(d) illustrates the change of the composition of the residual oil of reservoirs in the four cases with the production time. During the depletion production stage, the component contents of the CH4 decrease in all four cases, while the contents of the other components increase. The percentage content of the heavier components (C5–C36) increases more and more, which is similar to the results of our previous study [38]. After 1600 days, the content of the hydrocarbon components decreased rapidly due to the injection

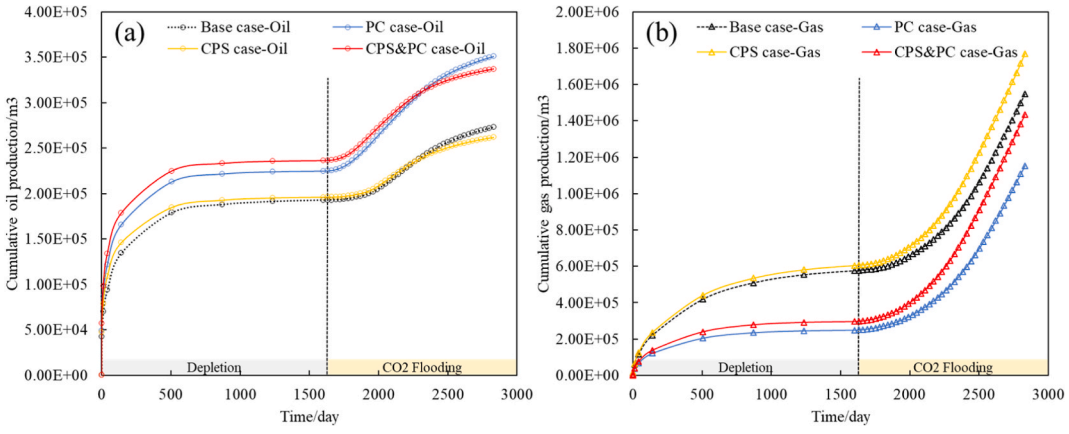

Fig. 12. Comparison of cumulative production with pore radius of 10 nm in the four models: (a) cumulative oil production; (b) cumulative gas production.

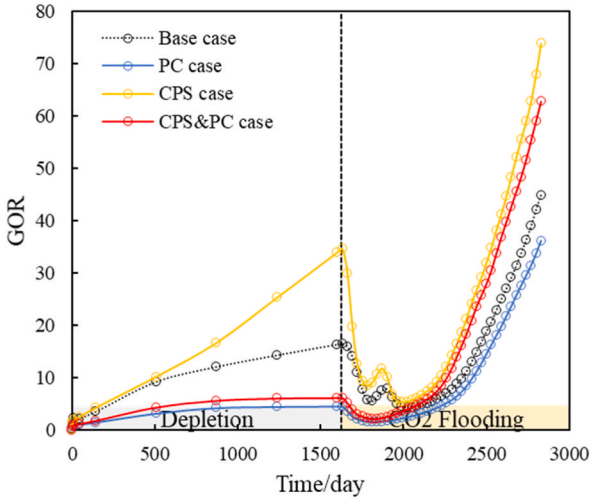

Fig. 13. Comparison of GOR with pore radius of 10 nm.

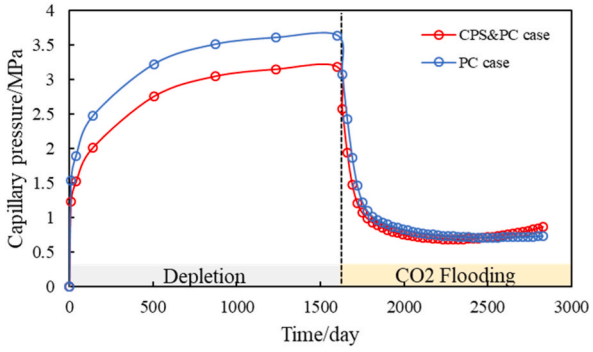

Fig. 14. Comparison of capillary pressure between PC case and CPS&PC case.

of CO2.

The residual oil component composition at the end of depletion production (Date 1600 days) is shown in Fig. 17. The residual oil composition of PC case and CPS&PC case were compared with Base case, and the results showed that the lighter components (CH4-NC4) of residual oil of PC and CPS&PC cases were 14.4% and 12.5% more than Base case, and the heavier components (C5–C36) were 14.7% and 12.7% less than Base case, respectively. The simulation results of CPS case are comparable to that of Base case, but the effects on light and heavy components are opposite to those of PC case and CPS&PC case. The lighter components (CH4-NC4) of residual oil of CPS cases were 1.3% less than base case, and the heavier components (C5–C36) were 1.4% more than base case.

As shown in Fig. 18 (a)-(d), crude oil is rapidly degassed at the initial time of depletion production. The composition of the residual gas is dominated by light components (CH4-NC4). With the depletion production going on, the CH4 content decreased, while the contents of other components increase in all four cases. Compared to the Base case, the reduction of CH4 in the residual gas composition is less in the PC and CPS&PC case, and the reduction of CH4 in the residual gas is greater in the CPS case. After 1600 days' production, the content of the hydrocarbon components decreased rapidly due to the injection of CO2. At the end of CO2 flooding, the CO2 content in the gas phase is close to 100%, which is caused by the breakthrough of CO2.

Fig. 19 illustrates the composition of the residual gas composition at the end of depletion production (the 1600th day). Under the initial conditions of the reservoir, the fluid is only oil and water, and the initial gas saturation is 0. The residual gas composition of PC and CPS&PC case were compared with Base case, and the results showed that CH4 of residual gas of PC case and CPS&PC cases were 8.7% and 5.6% higher than Base case, and C2-NC4 were 7.8% and 5.5% lower than Base case, respectively. The CH4 of residual gas of CPS cases were 2.9% lower than Base case, and the C2-NC4 were 1.9% higher than Base case.

From our perspective, the concept of the mechanism for fluid phase behavior in the dual pore structure of tight reservoir is shown in Fig. 20. There are bulk spaces (fractures) and nano spaces (nanopores) in tight hydraulic fracturing systems. Instead of considering the critical properties shift effect and capillary force effect in fractures (Base case) , the critical properties shift effect (CPS case) or capillary force effect (PC case) or the coupling of the two effects (CPS&PC case) are considered in nanopores. At reservoir temperature, as the formation pressure decreases with production (Step 1), the crude oil in the fractures begins to be degassed, but the bubble point pressure in the nanopore is lower than the pressure in the fracture and oil has not yet degassed due to the influence of critical properties

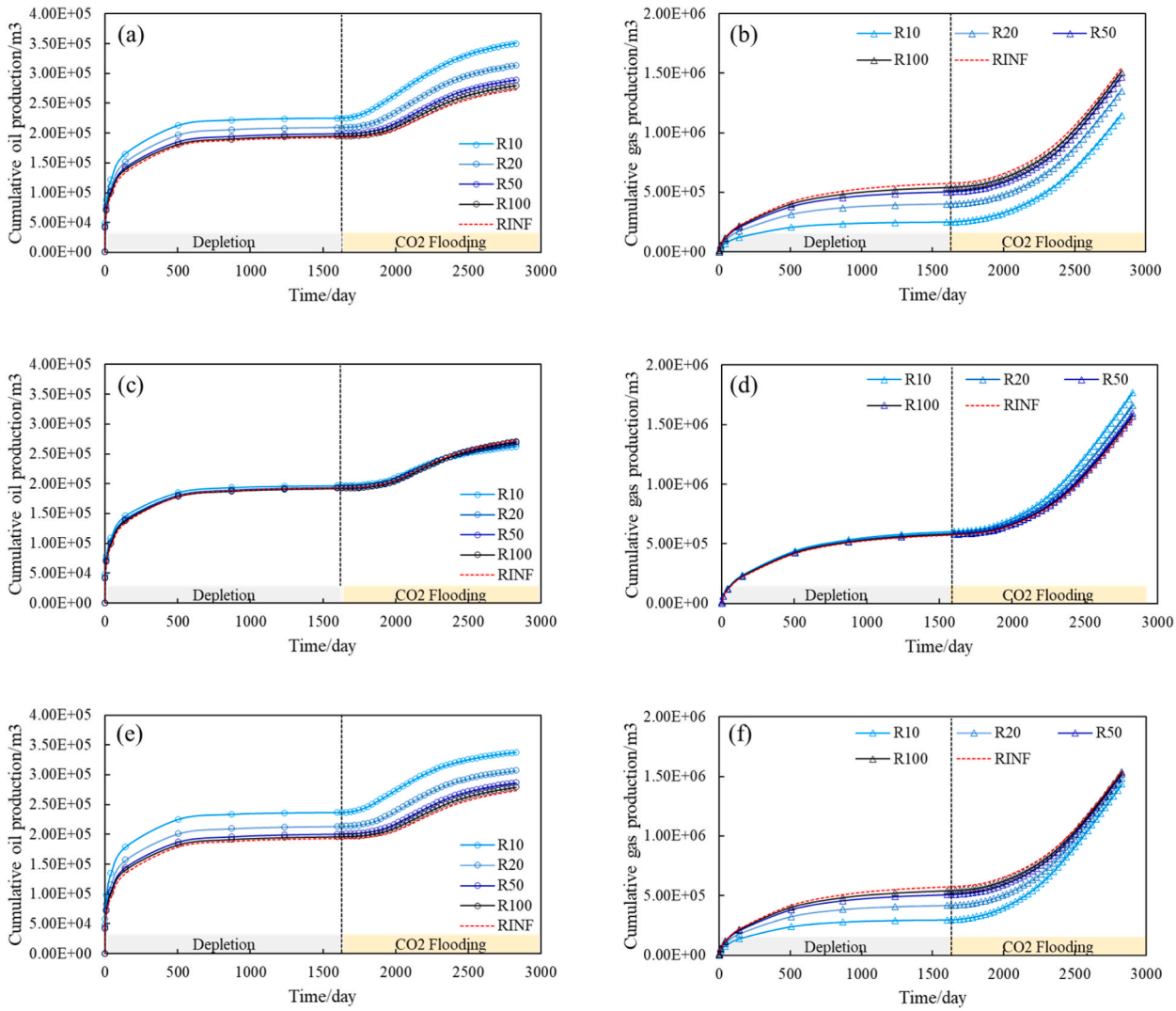

Fig. 15. Comparison of cumulative oil/gas production of PC case, CPS case and CPS&PC case under different pore radius: (a)cumulative oil production of PC case; (b)cumulative gas production of PC case; (c) cumulative oil production of CPS case; (d)cumulative gas production of CPS case; (e)cumulative oil production of PC& CPS case; (f)cumulative gas production of PC& CPS case.

shift and capillary pressure effect on fluid phase behavior. After the formation pressure continues to drop (Step 2), the CPS case in the nanopore that considers only the critical properties starts to degas. After the formation pressure is reduced lower (Step 3), the cases considering only the capillary pressure and coupling effects degasses due to the effect of capillary pressure on fluid phase behavior. Furthermore, in nanopores, the critical properties shift effect will lead to more light components from the oil phase transferred to the vapor phase and produce more gas. The residual oil of PC case and CPS&PC case have more light components and less heavy components than CPS case, which is consistent with the lower oil saturation of the reservoir grids and the higher cumulative gas production shown in Fig. 10(a). This indicates that capillary pressure displays a more positive effect on oil production, resulting in an increase in light components in the residual oil phase, which means more oil can be recovered. Moreover, the capillary pressure effect exhibits a more significant influence on the production compared to the critical shift effect.

This work presented a theoretical result that represents the complex pore system in real reservoirs with homogeneous pore size, ignoring the geological properties. Subsequently, the complexity of reservoir pores will be involved into simulation of real reservoir rocks, which certainly would be a challenge to perform and interpret phase behavior with the consideration of critical pressure and property shift effects.

5. Conclusions

The shift of confined fluid phase behavior in nanopores have been long recognized and widely accepted by the academic

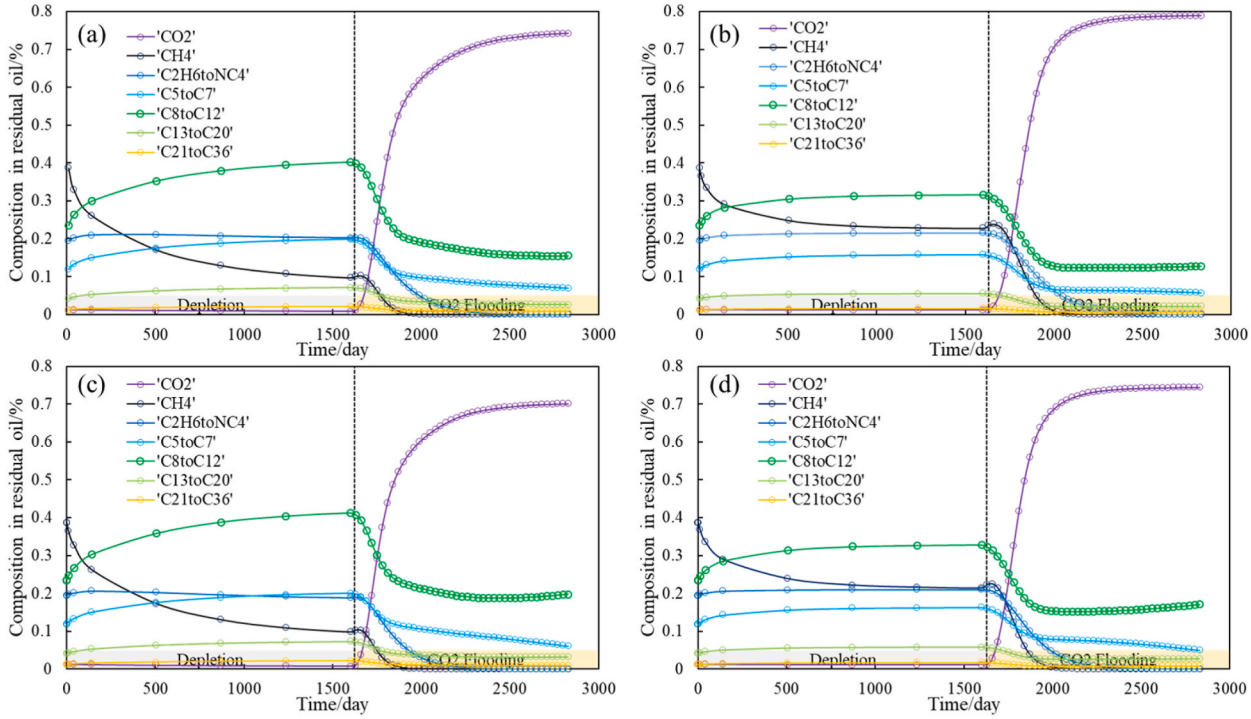

Fig. 16. (a) Residual oil composition in Base case with pore radius of 10 nm; (b) Residual oil composition in PC case with pore radius of 10 nm; (c) Residual oil composition in CPS case with pore radius of 10 nm; (d) Residual oil composition in CPS&PC case with pore radius of 10 nm.

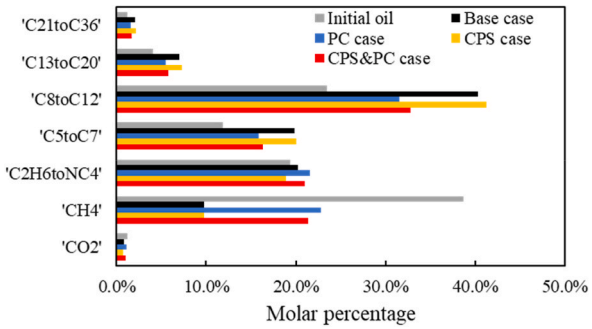

Fig. 17. Comparison of composition of residual oil in reservoir after 1600 days of production with pore radius of 10 nm.

community, however, at the current stage, current simulators are unable to fully explore this phenomenon. In this work, a novel fully compositional numerical simulation algorithm considering effect of critical properties shift and capillary pressure on phase behavior is accomplished. Based on the fully compositional numerical simulation, we have discussed the alterations of critical properties shift effect, capillary pressure effect and coupling effect on the composition of oil and gas production in detail. The critical properties shift and capillary pressure effects on oil and gas production in tight reservoirs are analyzed quantitatively through four cases, and the influences of the two effects in oil/gas production are compared. The main conclusions of this work are as follows:

- The novel fully compositional simulator results that consider coupling effects are more favourable to oil production than common simulator results, with a 23.5% difference in the cumulative oil production between the two results. Further, the simulation results considering the coupling effect have a lower production gasoline ratio. It is more suitable for simulating the production development of tight reservoirs.
- The capillary pressure effect is more important and dominate in terms of reservoir saturation and cumulative production in comparison with the critical properties shift effect. Through the quantitative comparison with Base case, the differences of oil/gas production between the two cases considered capillary pressure effect and Base case are much larger than that between the critical properties shift effect and Base case.

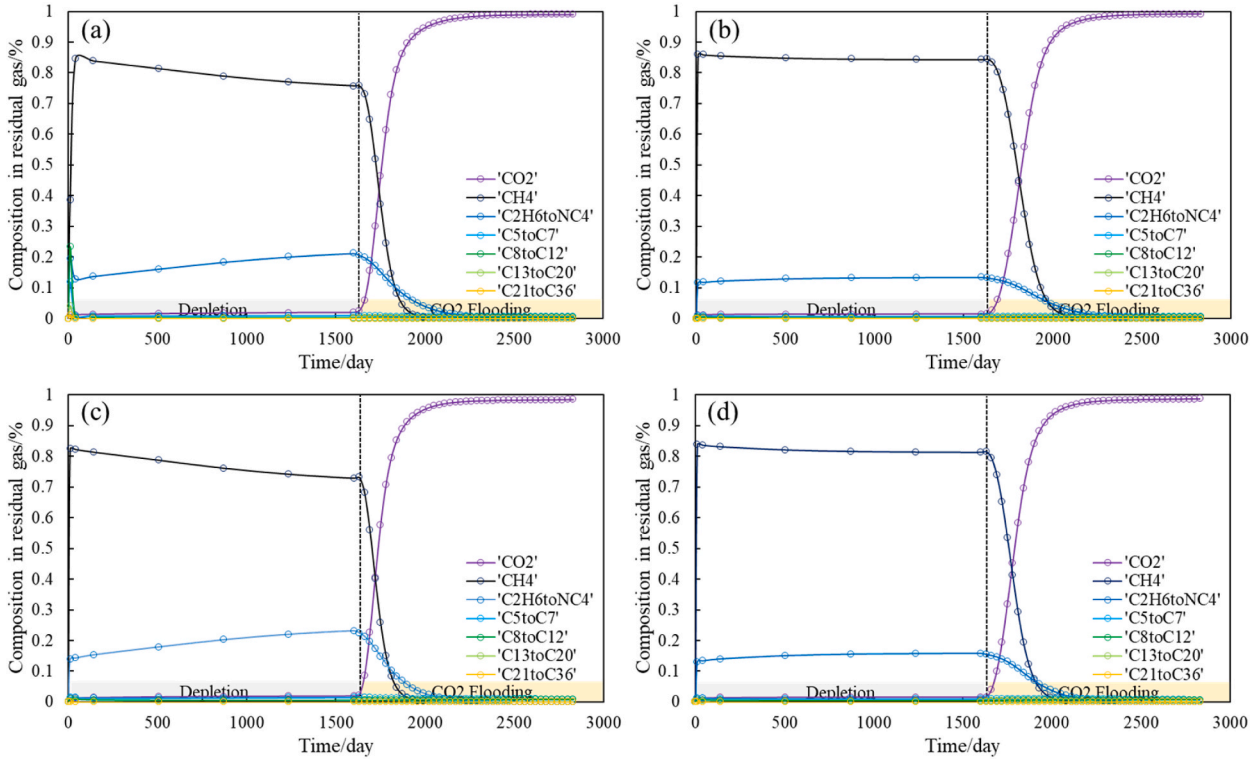

Fig. 18. (a) Residual gas composition in Base case with pore radius of 10 nm; (b) Residual gas composition in PC case with pore radius of 10 nm; (c) Residual gas composition in CPS case with pore radius of 10 nm; (d) Residual gas composition in CPS&PC case with pore radius of 10 nm.

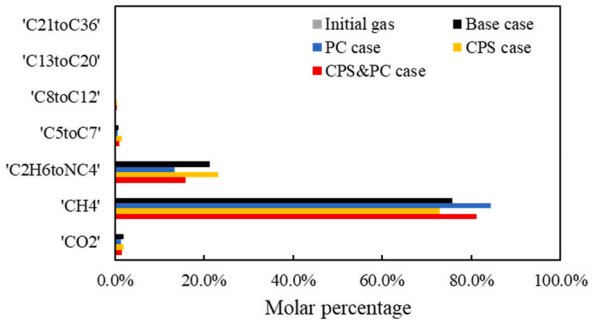

Fig. 19. Comparison of composition of residual gas in reservoir after 1600 days of production with pore radius of 10 nm.

- Confined effect has a significant impact on oil and gas production in pores narrower than 50 nm. The decrease of pore radius has a significant effect on the cumulative hydrocarbon production, and compared with critical properties, the capillary pressure is more sensitive to pore size.
- As oil and gas production proceeds, the composition of the fluid in the reservoir is constantly changing. In nanopores, the critical properties shift effect will lead to more light components transferred from the oil phase to the vapor phase and thus produce more gas. However, capillary pressure effect leads to a reduction in light components and an increase in heavy components in the residual oil/gas.

Author contribution statement

Yuhua Ma: Conceived and designed the experiments; Performed the experiments; Analyzed and interpreted the data; Wrote the paper.

Zhihong Kang; Xiaodong Chen; Congbo Gou; Zhijiang Kang: Contributed reagents, materials, analysis tools or data.

Xin Lei: Conceived and designed the experiments; Wrote the paper.

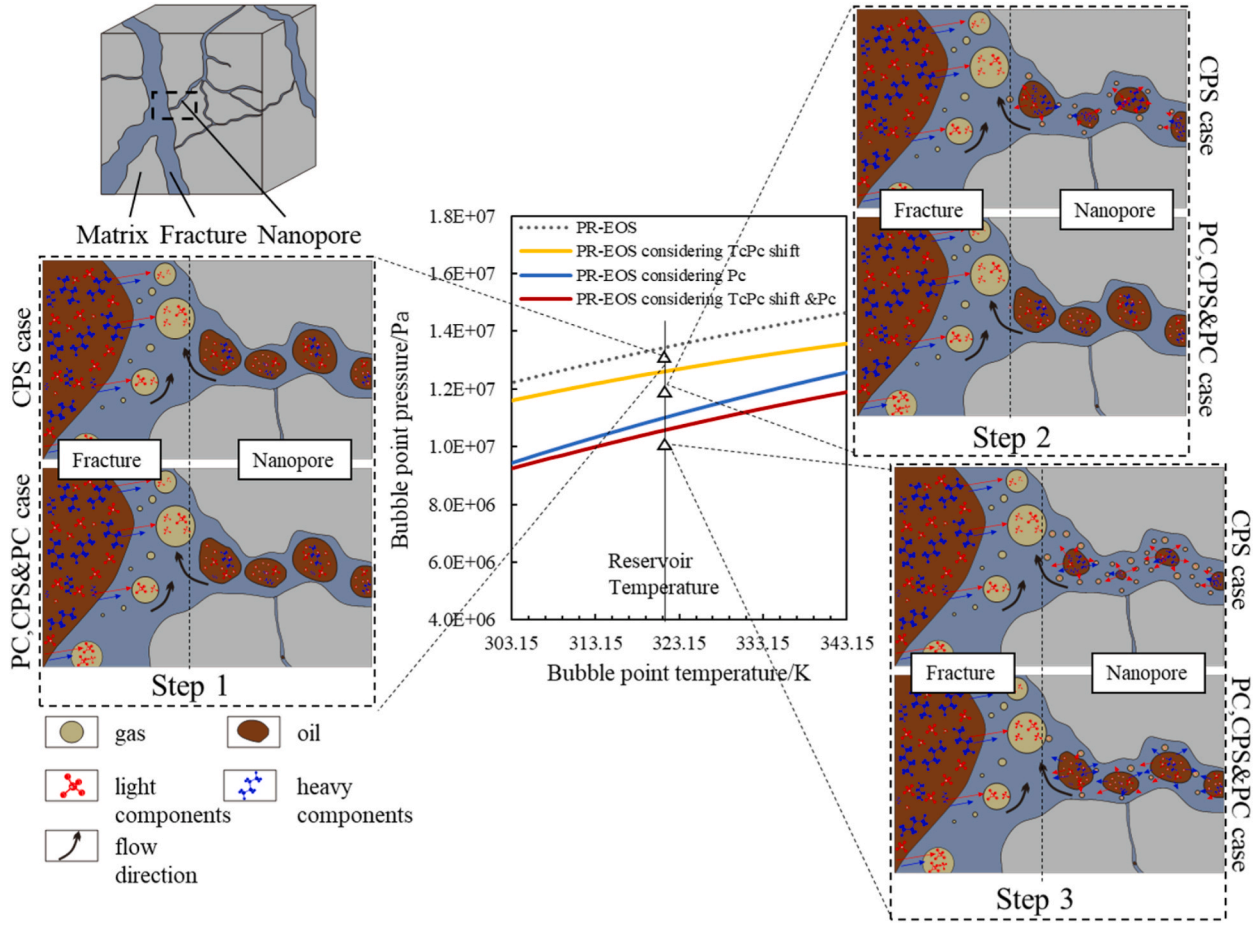

Fig. 20. Conceptual mechanism for fluid phase behavior in the dual pore structure of tight reservoir. The red Molecular Model represents the lighter components and the blue Molecular Model represents the heavier components. The red line represents the lighter components transferred from the oil phase to the vapor phase, and the blue line represents the heavier components transferred from the oil phase to the vapor phase. (For interpretation of the references to color in this figure legend, the reader is referred to the Web version of this article.)

Shuoliang Wang: Conceived and designed the experiments; Analyzed and interpreted the data.

Data availability statement

Data included in article/supp. material/referenced in article.

Declaration of competing interest

The authors declare that they have no known competing financial interests or personal relationships that could have appeared to influence the work reported in this paper.

Acknowledgement

This work was supported by the Joint Fund for Enterprise Innovation and Development of NSFC (Grant No. U19B6003).

Nomenclature

a	parameter of PR-EOS
b	parameter of PR-EOS
d	pore diameter
f_l	fugacity of component i in the liquid phase
fv	fugacity of component i in the vapor phase

K_{rg}	relative permeability of gas phase
K_{rl}	relative permeability of liquid phase
K_{ro}	relative permeability of oil phase
K_{rw}	relative permeability of water
P_c	critical pressure of confined fluids(atm)
P_{cap}	capillary pressure
P_{cb}	critical pressure of bulk fluids
P_l	liquid pressure
P_v	vapor pressure
R	gas constant
r_p	pore radius
S_l	liquid saturation
S_w	water saturation
T	reservoir temperature
T_c	critical temperature of confined fluids
T_{cb}	critical temperature of bulk fluids
V	molar volume
w	acentric factor of component i
x_i	mole fraction of component i in the vapor phase
y^i	mole fraction of component i in the liquid phase
Z_L	compressibility factor for liquid phase
Z_V	compressibility factor for vapor phase
σ	interfacial tension between vapor and liquid phase
θ	contact angle
ω_i	acentric factor
δ_{ij}	the binary interaction coefficient of components i and j
P_i	parachor of liquid/vapor phases
$\overline{\rho}_{L/V}$	molar density of bulk liquid/vapor phases
$\varnothing_L^i$	fugacity coefficient of liquid phases for a mixture
$\varnothing_V^i$	fugacity coefficient of vapor phases for a mixture
f	fugacity
$\Delta\ T_c$	shift of the critical temperature
$\Delta\ P_c$	shift of the critical pressure

References

[1] D.J. Soeder, S.J. Borglum, The Fossil Fuel Revolution: Shale Gas and Tight Oil, Elsevier, 2019.

[2] C. Jia, M. Zheng, Y. Zhang, Unconventional hydrocarbon resources in China and the prospect of exploration and development, Petrol. Explor. Dev. 39 (2) (2012) 139–146, https://doi.org/10.1016/S1876-3804(12)60026-3.

[3] S.H. Stevens, K.D. Moodhe, V.A. Kuuskraa, China shale gas and shale oil resource evaluation and technical challenges, in: SPE Asia Pacific Oil and Gas Conference and Exhibition, 2013, https://doi.org/10.2118/165832-MS.

[4] M.T. Le, An assessment of the potential for the development of the shale gas industry in countries outside of North America, Heliyon 4 (2) (2018), e00516, https://doi.org/10.1016/j.heliyon.2018.e00516.

[5] O. Arogundade, M. Sohrabi, A review of recent developments and challenges in shale gas recovery, in: SPE Saudi Arabia Section Technical Symposium and Exhibition, 2012, https://doi.org/10.2118/160869-MS.

[6] L. Du, L. Chu, L. Du, L. Chu, Understanding anomalous phase behavior in unconventional oil reservoirs, in: SPE Canadian Unconventional Resources Conference, 2012, https://doi.org/10.2118/161830-MS.

[7] B. Nojabaei, R.T. Johns, L. Chu, Effect of capillary pressure on phase behavior in tight rocks and shales, SPE Reservoir Eval. Eng. 16 (3) (2013) 281–289, https://doi.org/10.2118/159258-PA.

[8] N.S. Alharthy, T. Nguyen, T. Teklu, H. Kazemi, R. Graves, Multiphase compositional modeling in small-scale pores of unconventional shale reservoirs, in: SPE Annual Technical Conference and Exhibition, 2013, https://doi.org/10.2118/166306-MS.

[9] L. Jin, Y. Ma, A. Jamili, Investigating the effect of pore proximity on phase behavior and fluid properties in shale formations, in: SPE Annual Technical Conference and Exhibition, 2013, https://doi.org/10.2118/166192-MS.

[10] Y. Zhang, F. Civan, D. Devegowda, R.F. Sigal, Improved prediction of Multi-component hydrocarbon fluid properties in organic rich Shale reservoirs, in: SPE Annual Technical Conference and Exhibition, 2013, https://doi.org/10.2118/166290-MS.

[11] Y.C. Yortsos, A.K. Stubos, Phase change in porous media, Curr. Opin. Colloid Interface Sci. 6 (3) (2001) 208–216, https://doi.org/10.1016/S1359-0294(01)00085-1.

[12] H. Sun, H.A. Li, A new three-phase flash algorithm considering capillary pressure in a confined space, Chem. Eng. Sci. 193 (2019) 346–363, https://doi.org/10.1016/j.ces.2018.09.013.

[13] R. Li, H.A. Li, Improved three-phase equilibrium calculation algorithm for water/hydrocarbon mixtures, Fuel 244 (2019) 517–527, https://doi.org/10.1016/j.fuel.2019.02.026.

[14] H. Li, Multiphase Equilibria of Complex Reservoir Fluids: an Equation of State Modeling Approach, Springer Nature, 2021.

[15] J. Ally, S.H. Molla, F. Mostowfi, Condensation in nanoporous packed beds, Langmuir : the ACS journal of surfaces and colloids 32 (18) (2016) 4494–4499, https://doi.org/10.1021/acs.langmuir.6b01056.

[16] S. Luo, J.L. Lutkenhaus, H. Nasrabadi, Confinement-induced supercriticality and phase equilibria of hydrocarbons in nanopores, Langmuir 32 (44) (2016) 11506–11513, https://doi.org/10.1021/acs.langmuir.6b03177.
[17] J. Zhong, J. Riordon, S.H. Zandavi, Y. Xu, A.H. Persad, F. Mostowfi, D. Sinton, Capillary condensation in 8 nm deep channels, J. Phys. Chem. Lett. 9 (3) (2018) 497–503, https://doi.org/10.1021/acs.jpclett.7b03003.
[18] P.M. Sigmund, P.M. Dranchuk, N.R. Morrow, R.A. Purvis, Retrograde condensation in porous media, Soc. Petrol. Eng. J. 13 (2) (1973) 93–104, https://doi.org/10.2118/3476-PA.
[19] A. Brusilovsky, Mathematical simulation of phase behavior of natural multicomponent systems at high pressures with an equation of state, SPE Reservoir Eng. 7 (1992) 117–122, https://doi.org/10.2118/20180-PA.
[20] L. Wang, E. Parsa, Y. Gao, J.T. Ok, K. Neeves, X. Yin, E. Ozkan, Experimental study and modeling of the effect of nanoconfinement on hydrocarbon phase behavior in unconventional reservoirs, in: SPE Western North American and Rocky Mountain Joint Meeting, 2014, https://doi.org/10.2118/169581-MS.
[21] G. Yang, Z. Fan, X. Li, Determination of confined fluid phase behavior using extended Peng-Robinson equation of state, Chem. Eng. J. 378 (2019), 122032, https://doi.org/10.1016/j.cej.2019.122032.
[22] L.D. Gelb, K.E. Gubbins, R. Radhakrishnan, M. Sliwinska-Bartkowiak, Phase separation in confined systems, Rep. Prog. Phys. 62 (12) (1999) 1573, https://doi.org/10.1088/0034-4885/63/4/501.
[23] T.W. Teklu, N. Alharthy, H. Kazemi, X. Yin, R.M. Graves, A.M. AlSumaiti, Phase behavior and minimum miscibility pressure in nanopores, SPE Reservoir Eval. Eng. 17 (3) (2014) 396–403, https://doi.org/10.2118/168865-PA.
[24] R. Evans, U.M.B. Marconi, P. Tarazona, Fluids in narrow pores: adsorption, capillary condensation, and critical points, J. Chem. Phys. 84 (4) (1986) 2376–2399, https://doi.org/10.1063/1.450352.
[25] M. Thommes, G.H. Findenegg, Pore condensation and critical-point shift of a fluid in controlled-pore glass, Langmuir 10 (11) (1994) 4270–4277, https://doi.org/10.1021/la00023a058.
[26] G. Günther, J. Prass, O. Paris, M. Schoen, Novel insights into nanopore deformation caused by capillary condensation, Phys. Rev. Lett. 101 (8) (2008), 086104, https://doi.org/10.1103/PhysRevLett.101.086104.
[27] K.E. Gubbins, Y. Long, M. Śliwinska-Bartkowiak, Thermodynamics of confined nano-phases, J. Chem. Therm. 74 (2014) 169–183, https://doi.org/10.1016/j.jct.2014.01.024.
[28] J.H. Yun, T. Düren, F.J. Keil, N.A. Seaton, Adsorption of methane, ethane, and their binary mixtures on MCM-41: experimental evaluation of methods for the prediction of adsorption equilibrium, Langmuir 18 (7) (2002) 2693–2701, https://doi.org/10.1021/la015585.
[29] M. Thommes, K.A. Cychosz, Physical adsorption characterization of nanoporous materials: progress and challenges, Adsorption 20 (2) (2014) 233–250, https://doi.org/10.1007/s10450-014-9606-z.
[30] Z. Song, Y. Song, J. Guo, Z. Zhang, J. Hou, Adsorption induced critical shifts of confined fluids in shale nanopores, Chem. Eng. J. 385 (2020), 123837, https://doi.org/10.1016/j.cej.2019.123837.
[31] Y. Song, Z. Song, D. Feng, J. Qin, Y. Chen, Y. Shi, K. Song, Phase behavior of hydrocarbon mixture in shale nanopores considering the effect of adsorption and its induced critical shifts, Ind. Eng. Chem. Res. 59 (17) (2020) 8374–8382, https://doi.org/10.1021/acs.iecr.0c00490.
[32] K. Zhang, N. Jia, Confined fluid interfacial tension calculations and evaluations in nanopores, Fuel 237 (2019) 1161–1176, https://doi.org/10.1016/j.fuel.2018.10.036.
[33] F. Casanova, C.E. Chiang, C.P. Li, I.V. Roshchin, A.M. Ruminski, M.J. Sailor, I.K. Schuller, Effect of surface interactions on the hysteresis of capillary condensation in nanopores, EPL (Europhysics Letters) 81 (2) (2007), 26003, https://doi.org/10.1209/0295-5075/81/26003.
[34] D.R. Cole, S. Ok, A. Striolo, A. Phan, Hydrocarbon behavior at nanoscale interfaces, Rev. Mineral. Geochem. 75 (1) (2013) 495–545, https://doi.org/10.2138/rmg.2013.75.16.
[35] L. Travalloni, M. Castier, F.W. Tavares, S.I. Sandler, Critical behavior of pure confined fluids from an extension of the van der Waals equation of state, J. Supercrit. Fluids 55 (2) (2010) 455–461, https://doi.org/10.1016/j.supflu.2010.09.008.
[36] S. Chen, J. Jiang, B. Guo, A pore-network-based upscaling framework for the nanoconfined phase behavior in shale rocks, Chem. Eng. J. 417 (2021), 129210, https://doi.org/10.1016/j.cej.2021.129210.
[37] M.M. Honarpour, N.R. Nagarajan, A. Orangi, F. Arasteh, Z. Yao, Characterization of critical fluid, rock, and rock-fluid properties-impact on reservoir performance of liquid-rich shales, in: SPE Annual Technical Conference and Exhibition, 2012, https://doi.org/10.2118/158042-MS.
[38] T. Firincioglu, C. Ozgen, E. Ozkan, An excess-bubble-point-suppression correlation for black oil simulation of nano-porous unconventional oil reservoirs, in: SPE Annual Technical Conference and Exhibition, 2013, https://doi.org/10.2118/166459-MS.
[39] Y. Wang, B. Yan, J. Killough, Compositional modeling of tight oil using dynamic nanopore properties, in: SPE Annual Technical Conference and Exhibition, 2013, https://doi.org/10.2118/166267-MS.
[40] N. Siripatrachai, T. Ertekin, R. Johns, Compositional simulation of discrete fractures incorporating the effect of capillary pressure on phase behavior, SPE Improved Oil Recovery Conference (2016), https://doi.org/10.2118/179660-MS.
[41] Y. Ma, S. Wang, Z. Kang, L. Zhao, A compositional numerical study in hydraulic fractured tight reservoir: considering capillary pressure in phase behavior calculation, J. Petrol. Sci. Eng. 196 (2021), 108071, https://doi.org/10.1016/j.petrol.2020.108071.
[42] L. Li, J.J. Sheng, Nanopore confinement effects on phase behavior and capillary pressure in a Wolfcamp shale reservoir, J. Taiwan Inst. Chem. Eng. 78 (2017) 317–328, https://doi.org/10.1016/j.jtice.2017.06.024.
[43] Y. Zhang, Y. Di, W. Yu, K. Sepehrnoori, A comprehensive model for investigation of carbon dioxide enhanced oil recovery with nanopore confinement in the Bakken tight oil reservoir, SPE Reservoir Eval. Eng. 22 (1) (2019) 122–136, https://doi.org/10.2118/187211-PA.
[44] S.K. Singh, A. Sinha, G. Deo, J.K. Singh, Vapor− liquid phase coexistence, critical properties, and surface tension of confined alkanes, J. Phys. Chem. C 113 (17) (2009) 7170–7180, https://doi.org/10.1021/jp8073915.
[45] K. Zhang, N. Jia, L. Liu, Generalized critical shifts of confined fluids in nanopores with adsorptions, Chem. Eng. J. 372 (2019) 809–814, https://doi.org/10.1016/j.cej.2019.04.198.
[46] K. Zhang, N. Jia, S. Li, L. Liu, Thermodynamic phase behaviour and miscibility of confined fluids in nanopores, Chem. Eng. J. 351 (2018) 1115–1128, https://doi.org/10.1016/j.cej.2018.06.088.
[47] G.J. Zarragoicoechea, V.A. Kuz, Critical shift of a confined fluid in a nanopore, Fluid Phase Equil. 220 (1) (2004) 7–9, https://doi.org/10.1016/j.fluids.2004.02.014.
[48] K. Morishige, H. Fujii, M. Uga, D. Kinukawa, Capillary critical point of argon, nitrogen, oxygen, ethylene, and carbon dioxide in MCM-41, Langmuir 13 (13) (1997) 3494–3498, https://doi.org/10.1021/la970079u.
[49] D.Y. Peng, D.B. Robinson, A new two-constant equation of state, Ind. Eng. Chem. Fundam. 15 (1) (1976) 59–64, https://doi.org/10.1021/i160057a011.
[50] D.B. Macleod, On a relation between surface tension and density, Trans. Faraday Soc. (1923;19(July) 38–41, https://doi.org/10.1039/TF9231900038.
[51] K.S. Pedersen, P.L. Christensen, J.A. Shaikh, P.L. Christensen, Phase Behavior of Petroleum Reservoir Fluids, CRC press, 2006, https://doi.org/10.1201/9781420018257.
[52] W.Y. Zhu, M. Yue, Y.F. Liu, K. Liu, Z. Song, Research progress on tight oil exploration in China, Chin. J. Eng. 41 (9) (2019) 1103, https://doi.org/10.13374/j.issn2095-9389.2019.09.001.
[53] K. Qian, S. Yang, H. Dou, Q. Wang, L. Wang, Y. Huang, Experimental investigation on microscopic residual oil distribution during CO2 Huff-and-Puff process in tight oil reservoirs, Energies 11 (10) (2018) 2843, https://doi.org/10.3390/en11102843.
[54] J. Zhao, J. Fan, Y. He, Z. Yang, W. Gao, W. Gao, Optimization of horizontal well injection-production parameters for ultra-low permeable–tight oil production: a case from Changqing Oilfield, Ordos Basin, NW China, Petrol. Explor. Dev. 42 (1) (2015) 74–82, https://doi.org/10.1016/S1876-3804(15)60008-8.
[55] K. Zhang, L. Liu, G. Huang, Nanoconfined water effect on CO2 utilization and geological storage, Geophys. Res. Lett. 47 (15) (2020), e2020GL087999, https://doi.org/10.1029/2020GL087999.